Acta Crystallographica Section D
Biological Crystallography
ISSN 0907-4449

Crystallization and X-ray diffraction analysis of an all-RNA $U_{39}C$ mutant of the minimal hairpin ribozyme

Valerie Grum-Tokars,[a] Michael Milovanovic[a] and Joseph E. Wedekind[b,a]*

[a]The Department of Biochemistry and Molecular Biology, FUHS/The Chicago Medical School, 3333 Green Bay Road, North Chicago, Illinois 60064, USA, and [b]The Department of Biochemistry and Biophysics, University of Rochester Medical Center, 601 Elmwood Avenue, Rochester, New York 14642, USA

Correspondence e-mail: joseph_wedekind@urmc.rochester.edu

Received 27 July 2002
Accepted 16 October 2002

The hairpin ribozyme is a naturally occurring catalytic RNA composed of two helix–loop–helix domains, *A* and *B*, that dock to form the biologically active enzyme. Previously, the crystal structure of the hairpin has been solved as a four-way helical junction that incorporated the U1A protein as an artificial crystal-packing motif [Rupert & Ferré-D'Amaré (2001), *Nature (London)*, **410**, 780–786]. Here, the crystallization of a minimal junctionless hairpin ribozyme 64-mer is reported in the absence of protein. Crystals grow in space group $P6_122$, with unit-cell parameters a = 93.1, c = 123.2 Å. Complete diffraction data have been collected to 3.35 Å resolution. Structural analysis should provide details of intermolecular RNA docking, including the ground-state conformations of the $U_{39}C$ mutation relevant to hairpin catalysis.

1. Introduction

Ribozymes comprise a functionally diverse group of RNA catalysts divisible into two families based on size. The large family includes self-splicing introns, RNase P and the ribosome. The small family includes the hepatitis δ virus, hammerhead, VS and hairpin ribozymes (McKay & Wedekind, 1999). Members of the small cohort are derived from subviral animal or plant pathogens, as well as satellite plasmids such as those of *Neurospora* and *Notophthalmus*. Small ribozymes share a common chemical mechanism that proceeds through a trigonal bipyramidal transition state yielding a cyclic 2′,3′-phosphodiester and a 5′-hydroxyl group as products (Fig. 1*a*). Such cleavage activity arose from the need to process rolling-circle replication intermediates that must be reduced to unit length.

Of the small ribozymes, the hairpin exhibits unique catalytic properties. Activity is relatively pH independent (in the range 4–9) with a reaction equilibrium constant close to unity ($K_{\rm ligate/cleave}$ = 4.4) for the minimal motif (Nesbitt *et al.*, 1997). Inner sphere metal-ion coordination is not required for catalysis, although low concentrations of $Co(NH_3)_6^{3+}$ or molar quantities of monovalent cations stimulate activity (Nesbitt *et al.*, 1997, 1999). These properties point to a general acid/base mechanism involving one or more functional groups of the RNA (Fig. 1*a*). Recent proton-inventory experiments demonstrate two protons in flight in the transition state (Pinard *et al.*, 2001), suggesting a concerted mechanism similar to RNase A (Matta & Vo, 1986).

The minimal catalytic motif of the hairpin ribozyme comprises two helix–loop–helix domains (Hampel & Tritz, 1989) that dock to form the active site (Fedor, 2000). Substrate binding occurs in the *A* domain, whereas the *B* domain contributes key residues essential for catalysis. The high avidity between the internal loops is demonstrated by the ability to recapitulate ribozyme activity from domains that have been physically separated at positions 14 and 15 (Fig. 1*b*) (Butcher *et al.*, 1995; Shin *et al.*, 1996). The interdomain K_d of this *trans* construct is 4.1 μM in the presence of $Co(NH_3)_6Cl_3$. Notably, $k_{\rm cat}$ is reduced by only a factor of 2 compared with the minimal junctioned variant (Butcher *et al.*, 1995; Hampel *et al.*, 1998).

A previous crystallographic study of a four-way junction (4WJ) hairpin ribozyme in complex with U1A provided the first atomic details of this ribozyme fold (Rupert & Ferre-D'Amare, 2001). Although the 4WJ favors ligation by 30–50 over cleavage (Fedor, 1999), the structure reveals the 2′-hydroxyl of G_8 to be poised for cleavage of the G_{+1} phosphoryl group. This observation led to two mechanistic proposals (Rupert & Ferre-D'Amare, 2001) featuring either (i) the N1 positions of G_8 and A_{38} as general acid/base catalysts or (ii) acid/base catalysis involving water activation by A_9 or A_{10}. However, in the 4WJ structure, N1 of A_{38} is 4.5 Å from the leaving group. Furthermore, nucleotide-analog interference mapping (NAIM) indicates A_{10}, but not A_{38}, is ionized during catalysis, thus supporting a mechanism whereby A_{10} electrostatically contributes to the transition state (Fig. 1*a*) (Ryder *et al.*, 2001). Given the 4WJ structure, it is unclear how A_{10} could influence transition-state stability without significant conformational adjustments (Ryder *et al.*, 2001).

To further explore the molecular determinants of hairpin ribozyme catalysis, we have crystallized a non-junctioned (NJ) minimal ribozyme in the absence of proteins (Fig. 1*b*). Our construct features the $U_{39}C$ mutation that increases catalytic efficiency by fourfold relative to the wild type (Joseph & Burke, 1993). Two crystal forms have been prepared that are amenable to X-ray crystallographic structure determination. This paper describes details of RNA purification, crystallization and preliminary crystallographic analyses.

2. Materials and methods

2.1. Materials

RNA strands were synthesized by either Dharmacon Research (Lafayette, CO, USA) or the Yale HHMI Biopolymer–Keck Foundation Biotechnology Resource Laboratory (New Haven, CT, USA). Chemicals were from Acrõs Organics with the following exceptions. Cacodylic acid, spermidine·4HCl, NaOH, $(NH_4)_2SO_4$ and $MgCl_2$ were from Fisher Scientific. Pentaerythritol propoxylate (PEP) and ethoxylate (PEE) were from Aldrich. Poly(ethylene) glycol (PEG) was from Fluka. The Natrix crystallization screen, jeffamine M600, siliconized 22 mm glass cover slips and VDX Plates were from Hampton Research. Cover slips were autoclaved prior to use. All water was autoclaved and originated from an UV/UF Nanopure Infinity System (Barnstead).

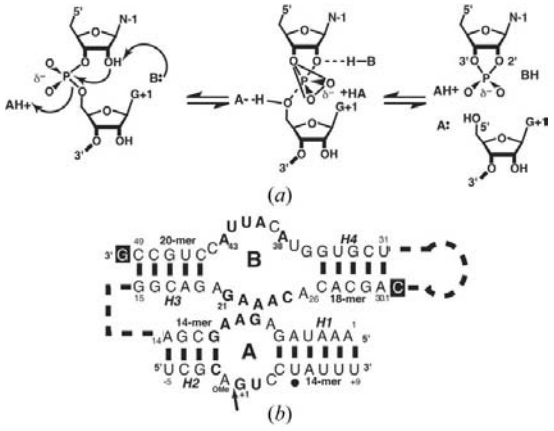

Figure 1
Reaction and secondary structure of the hairpin ribozyme. (*a*) The general acid/base mechanism of the hairpin ribozyme. (*b*) Schematic depiction of the minimal hairpin ribozyme constructs used in this study; conserved residues are in bold type. Blunt as well as overhanging or 'sticky' ends (black boxes) were screened in crystallization experiments. Dashed lines joining nucleotides 14 to 15 and 30.1 to 31 represent the phosphodiester linkage of junctioned constructs and a stem-loop, respectively; both features are absent in the ribozyme of this study. An arrow indicates the site of phosphodiester bond cleavage. Vertical bars are Watson–Crick hydrogen bonds. A 2′-*O*-methyl group has been incorporated at position A_{-1} to prevent bond cleavage. A black dot represents the site of 5-iodouracil incorporation for form II crystals.

2.2. RNA purification

Dharmacon oligonucleotides were deprotected per the manufacturer's instructions, except that heating was for 1 h at 338 K. Work-up of Yale strands was as described previously (Wedekind & McKay, 2000). RNA strands containing either 5-iodo- or 5-bromouracil were prepared and handled as described in Wedekind & McKay (2000). Individual RNA strands were purified by use of a 1.9 × 30 cm µBondapack C18 column (Waters) on a Waters HPLC equipped with Model 510 pumps, an automated gradient controller and a Waters 484 MS Absorbance Detector. HPLC separations employed the TEA/TEAA (triethylammonium acetate) ion-pairing system at pH 7.0. Buffer *A* was 0.10 *M* TEA/TEAA; buffer *B* comprised buffer *A* plus 50%(*v*/*v*) acetonitrile. Preparative-scale RNA separations were eluted at 7 ml min^{-1} with linear gradients using 15–30%(*v*/*v*) buffer *B* over 60 min intervals; Fig. 2 shows an analytical run. RNA elution was monitored at 260 nm; appropriate fractions were pooled and lyophilized to 1–2 ml volumes. Concentrated RNA was desalted using Sep Pak Vac C18 cartridges (Waters), which entailed loading, washing with water and batch elution with 40%(*v*/*v*) aqueous acetonitrile. HPLC and desalting have been described previously (Wedekind & McKay, 2000). Individual strands of desalted RNA were lyophilized to dryness, resuspended in 10 m*M* sodium cacodylate buffer pH 6.0 to a final working concentration of 1 m*M* and stored at 253 K until needed. The composition of desalted strands was verified by MALDI–TOF mass spectrometry at the Pan Facility (Stanford, CA, USA).

2.3. Crystal screening

Docked hairpin ribozyme complexes were prepared as follows. Precise molecular weights and extinction coefficients were calculated by use of the program *RNA2MW* (Wedekind, unpublished work). The *A* and *B* domains were formed separately by mixing equimolar quantities of 1 m*M* RNA strands; duplex mixtures were incubated for 30 min at 293 K. The ribozyme complex was recapitulated by mixing the respective 0.5 m*M* complexes of *A* and *B* together in a 1:1 molar ratio followed by the dropwise addition of 25 m*M* $Co(NH_3)_6Cl_3$ or $MgCl_2$ with vortexing. 14 complexes with variable-length *A* and *B* stems were tested for crystallization. *A* domains were kept blunt with strands ranging in size from 11- to 14-mers. Strands of the *B* domain were prepared with blunt, sticky or mixed (blunt and sticky) end compositions. Both 5′- and 3′-overhangs (Fig. 1*b*) were tested. Strands of the *B* domain ranged in size from 15- to 19-mers paired with 17- to 21-mers. Individual complexes were utilized immediately in crystallization trials and could not be stored frozen.

Crystallization screens were conducted by use of the hanging-drop vapor-diffusion method. A volume of 1 µl precipitating agent from a 1 ml reservoir was added to 1 µl of RNA. Duplicate trials were conducted at 277 and 293 K buffered at pH 6.0 with 50–100 m*M* sodium cacodylate. Salt precipitants included combinations of Li^+, Na^+, K^+, NH_4^+ and Mg^{2+} with counter ions Cl^-, SO_4^{2-}, malonate, tartrate and acetate. Organic precipitants included 2-propanol, ethanol, 2-methyl-2,4-pentanediol (MPD), 1,6-hexanediol, PEP, PEE (Gulick *et al.*, 2002), PEG, PEG monomethyl ether (PEG MME) and Jeffamine M600 pH 7. The latter five compounds were tested in combination with inorganic salts. All trials included 0.5–3 m*M* $Co(NH_3)_6Cl_3$ or 10–50 m*M* Mg^{2+}, as well as 2–10 m*M* spermidine or spermine. Additional trials were conducted using the Natrix Screen. Droplets were examined 3–6 d after setup by use of a dissecting microscope.

2.4. Crystal composition by HPLC analysis

Working under a dissecting microscope, several single crystals were removed from hanging drops by use of a glass Pasteur

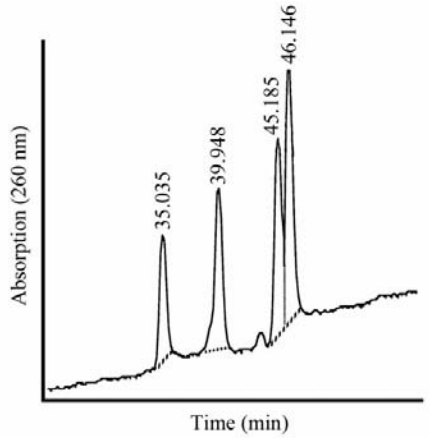

Figure 2
Reverse-phase chromatography trace of washed 64-mer hairpin ribozyme crystals. Peaks correspond to the respective 14-mer ribozyme and substrate strands of the *A* domain, followed by the 17-mer and 19-mer strands of the *B* domain.

pipette with a drawn-out tip. Crystals were transferred to a microfuge tube containing 50 µl synthetic mother liquor. The tube was spun briefly (14 000 rev min^{-1}) to sediment crystals. The synthetic mother liquor was exchanged with 3 × 50 µl washes, then drained to 5–10 µl with a filter-paper wick. Washed crystals were dissolved in 25 to 50 µl water, followed by heating to 338 K. The sample was microfuged for 1 min at maximum speed and then loaded into an HPLC sample loop with a Hamilton Syringe. Strand retention times and peak integration areas were assessed by use of the Dynamax MacIntegrator package (Varian).

2.5. X-ray diffraction experiments

As an initial assessment of crystal diffraction, samples were mounted in thin-walled quartz capillaries (Charles Supper) and analyzed in-house for X-ray diffraction. Intensities were recorded on a SMART 6000 CDD (Bruker AXS) equipped with three-circle geometry and confocal optics. Copper X-rays were generated by an RU-H3R rotating-anode generator (Rigaku/MSC) operated at 5.0 kW with a 300 µm focal spot. Promising crystals were cryoprotected through serial adaptations into synthetic mother liquor containing successively higher concentrations of glycerol (5–25%). Crystals were mounted in 20 µm rayon loops (Hampton Research) and flash-cooled by plunging directly into liquid nitrogen or by exposure to a stream of cold nitrogen gas at 100 K (Oxford Cryosystems). Diffraction data were recorded at a distance of 7 cm as 0.15° rotations per 360 s. Data were reduced by use of the *SMART*, *SAINT* and *PROSCALE* packages (Bruker AXS). Pre-screened crystals were removed from the goniometer by use of 18 mm cryotongs (Hampton Research) and stored in liquid nitrogen.

Synchrotron-based X-ray diffraction data were recorded on a Quantum 4 CCD detector (ADSC) on the bending-magnet beamline of Sector 14C at the Advanced Photon Source (Argonne, IL, USA). Whole data sets were recorded from single crystals. Owing to the radiation damage apparent from the scale factors, crystals were translated along the spindle axis as necessary. High-resolution data were recorded at a distance of 280 mm as 40 × 1° or 75 × 1° oscillations for form I and II crystals, respectively; c^* was oriented along the spindle axis, but offset by >10°. Exposure times were 180 s °$^{-1}$. Low-resolution passes were recorded at a distance of 370 mm as 2° oscillations; the beam path was purged with He gas. Exposure times were 5–10 s °$^{-1}$. Intensities were reduced and merged with *DENZO*/*SCALEPACK* (Otwinowski & Minor, 1997).

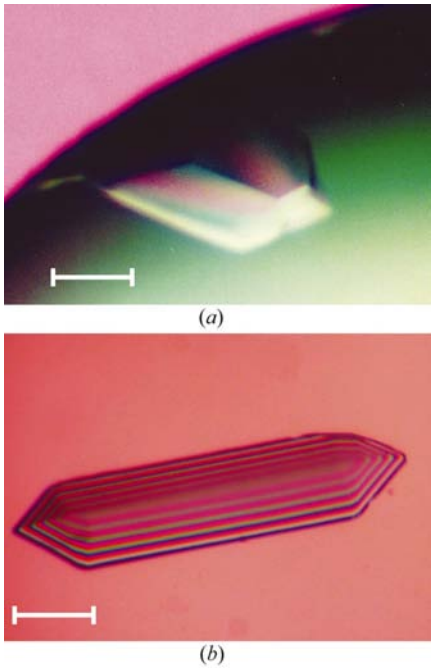

Figure 3
Photographs of the best all-RNA hairpin ribozyme crystals recorded under polarized light. (*a*) The 64-mer blunt-ended construct with dimensions 0.23 × 0.23 × 0.3 mm; the white bar is 115 µm. (*b*) The 66-mer construct with overhanging ends. Crystal dimensions are 0.35 × 0.35 × 1.6 mm; the white bar is 300 µm.

3. Results and discussion

3.1. Crystallization results

The choice of non-junctioned (NJ) crystallization constructs (Fig. 1*b*) avoids misfolding problems associated with 1WJ (one-way junction) or 2WJ ribozyme constructs in which position −5 is covalently linked to position 50 (Fedor, 1999; Walter *et al.*, 1999). NJ ribozymes are active, albeit with a K_m increase of nearly 10^4-fold (Butcher *et al.*, 1995). To avoid other misfolding problems, a *B* domain devoid of an H4 stem-loop (Fig. 1*b*) was chosen. This deletion circumvents intermolecular dimerization artifacts associated with RNA stem-loop crystallization (Baeyens *et al.*, 1996).

Based upon an empirical examination of more than 14 constructs (data deposited in the Biological Macromolecule Crystallization Database), we conclude that hairpin ribozyme crystallization is influenced greatly by the length of stems H3 and H4 in the *B* domain. Crystals appeared mostly between 1.5 and 2.5 *M* ionic strength including the Li^+, Na^+, K^+, NH_4^+ salts of malonate at pH 7 (data not shown); to our knowledge, malonate has been utilized previously only in protein crystallization (McPherson, 2001). Of the high-salt crystals observed, those grown from a blunt-ended 64-mer produce a superior hexagonal habit (Fig. 3*a*). These crystals (form I) can be prepared from solutions of 1.8 *M* ammonium sulfate, 2 m*M* spermidine and 0.1 *M* sodium cacodylate pH 6.0. The subtle addition of sticky ends to the *B* domain of form I crystals produces a trigonal crystal habit (form II; see Fig. 3*b*). The latter crystals are obtained from 1.3 *M* Li_2SO_4, 2 m*M* spermine and 0.1 *M* sodium cacodylate pH 6.0. Neither crystal form requires $Co(NH_3)_6Cl_3$ for growth, although the inclusion of 2.5 m*M* $Co(NH_3)_6Cl_3$ improves X-ray diffraction significantly. Both crystal forms were prepared from 0.25 m*M* NJ RNA concentrations at 293 K and reach full size within 3–4 weeks.

3.2. Crystal composition

The strand composition and RNA stoichiometries of form I and II crystals were assessed by HPLC. A mixture of all four RNA strands can be resolved under analytical conditions (Fig. 2). Elution standards were devised from pre-crystallization RNA stocks mixed with synthetic mother liquor. Control HPLC analyses were performed for individual RNA strands, as well as the pre-crystallization *AB* complex. The control results (data not shown) corroborate the strand composition and stoichiometries of crystals in terms of retention times and peak-integration areas. This methodology provides a fast inexpensive alternative to mass spectrometry of RNA and avoids the spectral complexity and overlap associated with high ionic strength. Even after six months, the RNA remains intact in crystals.

3.3. Diffraction results

Space-group assignments for form I and form II crystals were made by the agreement of reflections measured in multiplicity (Table 1) and by the systematic absences of type $l \neq 6n$ or $l \neq 3n$ for reflections of type 00*l*, respectively. Form I crystals belong to the hexagonal space group $P6_122$ (or enantiomer), with unit-cell parameters a = 94.0, c = 123.0 Å. The R_{sym} for the 64-mer is 6.8% (39.3%) from 3.35 to 30 Å resolution (Table 1) with an $I/\sigma(I)$ cutoff of −3. X-ray diffraction from form I crystals is relatively isotropic (Fig. 4). These crystals are better ordered than form II crystals despite their smaller size (Fig. 3*a*). Form II crystals grow as long trigonal prisms (Fig. 3*b*). Despite their large size, form II crystals diffract

Table 1
X-ray diffraction intensity statistics from the 64-mer and 66-mer crystals.

Values in parentheses correspond to reflections in the highest resolution shell.

	Form I (64-mer)	Form II (66-mer)
λ (Å)	1.0	1.0
Space group	$P6_122$ or $P6_522$	$P3_112$ or $P3_212$
Unit-cell parameters (Å)	$a = b = 93.1$, $c = 123.2$	$a = b = 76.1$, $c = 142.2$
Resolution range (Å)	3.35–30.0	4.30–30.0
Measured reflections	108536	56168
Unique reflections	5138	3035
Theoretical reflections	5223	3486
Completeness (%)	97.8 (90.1)	90.5 (81.9)
R_{sym}† (%)	6.8 (39.3)	7.9 (26.7)
$I/\sigma(I)$	32.9 (4.5)	21.2 (5.1)

† $R_{sym} = [\sum |I(h)_j - \langle I(h)\rangle| / \sum I(h)_j] \times 100$, where $I(h)_j$ is the observed intensity of the jth measurement of reflection h and $\langle I(h)\rangle$ is the mean intensity of reflection h.

anisotropically with a maximum resolution of 3.1 Å along c^*, but only 4.5 Å resolution along a^*. R_{sym} values are 7.9% (26.7%) from 4.3 to 30 Å resolution (Table 1). The solvent content of the respective crystal forms is estimated to be 65 and 78%, with one molecule per asymmetric unit. Based upon solvent considerations, two molecules are possible for form II crystals (55%), although both crystal forms are fragile and temperature sensitive. Weak diffraction and radiation sensitivity (based on relative scale factors; data not shown) indicate high solvent contents are likely for both crystal forms. Notably, iodination and bromination of individual uracil bases within the 66-mer improves the diffraction and lowers the anisotropy relative to the native. Marked improvements in diffraction were observed with halogenation at positions U_4 of the ribozyme strand, as well as positions +2, +5 and +7 of the substrate strand (Fig. 1*b*). Improved diffraction may be attributed to increased molecular crowding, although no dramatic changes are observed in unit-cell parameters compared with the native crystals. Notably, the structure determination of the 4WJ utilized 5-iodouracil at position +5, which lead to an improvement in diffraction relative to the SeMet-substituted U1A–RNA complex (Rupert & Ferre-D'Amare, 2001). In contrast, bromination of NJ positions 34, 37 and 46 of the *B* domain 20-mer altered the form II habit, resulting in crystals

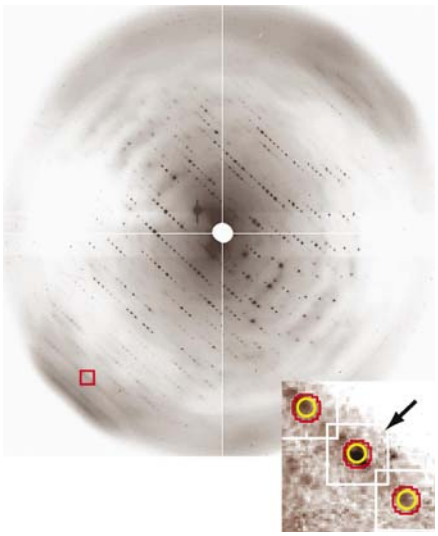

Figure 4
Representative X-ray diffraction pattern for the 64-mer blunt-ended hairpin ribozyme construct. The part in the red box is enlarged in the inset and shows Bragg diffraction at 3.45 Å resolution (arrow). Predicted reflections (yellow) from *XDISP*/*DENZO* overlay the experimental diffraction pattern.

of smaller size and poorer diffraction properties. The crystallization of constructs modified at position 37 relies heavily upon optimizing the concentration of polyamines, Mg^{2+} and RNA, which are factors important in tRNA crystallization (Dock-Bregeon & Moras, 1992). In the 4WJ crystal structure, the 5-position of the U_{37} base points away from the catalytic core, shielding its phosphate group from solvent. Thus, halogenation at this position is not expected to influence the local structure. Tb^{III} cleavage analysis of the $U_{39}C$ mutant indicates that U_{37} is a major target site (Walter *et al.*, 2000). Hence in the $U_{39}C$ mutant, the U_{37} phosphate may not be protected from solvent as seen in the 4WJ structure. At present, efforts are under way to solve the structure of the blunt-ended all-RNA $U_{39}C$ mutant of the hairpin ribozyme (crystal form I). Promising molecular-replacement solutions for crystal form II have been obtained.

This work was supported by American Cancer Society (IL Division) award No. 00-021, as well as NIH Grants GM63162 and RR15934 to JEW. The authors thank CLK for comments on the manuscript, as well as assistance from members of the BioCARS staff at the Advanced Photon Source. Use of the Advanced Photon Source was supported by the US Department of Energy, Basic Energy Sciences, Office of Science under Contract No. W-31-109-Eng-38. Use of the BioCARS Sector 14 was supported by the National Institutes of Health, National Center for Research Resources under grant No. RR07707.

References

Baeyens, K. J., De Bondt, H. L., Pardi, A. & Holbrook, S. R. (1996). *Proc. Natl Acad. Sci. USA*, **93**, 12851–12855.
Butcher, S. E., Heckman, J. E. & Burke, J. M. (1995). *J. Biol. Chem.* **270**, 29648–29651.
Dock-Bregeon, A.-C. & Moras, D. (1992). *Crystallization of Nucleic Acids and Proteins: A Practical Approach*, edited by A. Ducruix & R. Giegé, pp. 145–74. Oxford University Press.
Fedor, M. J. (1999). *Biochemistry*, **38**, 11040–11050.
Fedor, M. J. (2000). *J. Mol. Biol.* **297**, 269–291.
Gulick, A. M., Horswill, A. R., Thoden, J. B., Escalante-Semerena, J. C. & Rayment, I. (2002). *Acta Cryst.* D**58**, 306–309.
Hampel, A. & Tritz, R. (1989). *Biochemistry*, **28**, 4929–4933.
Hampel, K. J., Walter, N. G. & Burke, J. M. (1998). *Biochemistry*, **37**, 14672–14682.
Joseph, S. & Burke, J. M. (1993). *J. Biol. Chem.* **268**, 24515–24518.
McKay, D. B. & Wedekind, J. E. (1999). *The RNA World*, edited by T. Cech, pp. 265–286. New York: Cold Spring Harbor Laboratory Press.
McPherson, A. (2001). *Protein Sci.* **10**, 418–422.
Matta, M. S. & Vo, D. T. (1986). *J. Am. Chem. Soc.* **108**, 5316–5318.
Nesbitt, S. M., Erlacher, H. A. & Fedor, M. J. (1999). *J. Mol. Biol.* **286**, 1009–1024.
Nesbitt, S. M., Hegg, L. A. & Fedor, M. J. (1997). *Chem. Biol.* **4**, 619–630.
Otwinowski, Z. & Minor, W. (1997). *Methods Enzymol.* **276**, 307–326.
Pinard, R., Hampel, K. J., Heckman, J. E., Lambert, D., Chan, P. A., Major, F. & Burke, J. M. (2001). *EMBO J.* **20**, 6434–6442.
Rupert, P. B. & Ferre-D'Amare, A. R. (2001). *Nature (London)*, **410**, 780–786.
Ryder, S. P., Oyelere, A. K., Padilla, J. L., Klostermeier, D., Millar, D. P. & Strobel, S. A. (2001). *RNA*, **7**, 1454–1463.
Shin, C., Choi, J. N., Song, S. I., Song, J. T., Ahn, J. H., Lee, J. S. & Choi, Y. D. (1996). *Nucleic Acids Res.* **24**, 2685–2689.
Walter, N. G., Burke, J. M & Millar, D. P. (1999). *Nature Struct. Biol.* **6**, 544–549.
Walter, N. G., Yang, N. & Burke, J. M. (2000). *J. Mol. Biol.* **298**, 539–555.
Wedekind, J. E. & McKay, D. B. (2000). *Methods Enzymol.* **317**, 149–168.